HHS Public Access

Author manuscript

*Nat Struct Mol Biol*. Author manuscript; available in PMC 2016 June 07.

Published in final edited form as:

*Nat Struct Mol Biol*. 2016 January ; 23(1): 31–36. doi:10.1038/nsmb.3138.

# Structural dynamics of potassium channel gating revealed by single molecule FRET

**Shizhen Wang**[#1], **Reza Vafabakhsh**[#2], **William F. Borschel**[1], **Taekjip Ha**[2,3,4,#], and **Colin G. Nichols**[1,#]

[1]Center for Investigation of Membrane Excitability Diseases, Department of Cell Biology and Physiology, Washington University School of Medicine, St. Louis MO

[2]Department of Physics and the Center for the Physics of Living Cells, University of Illinois at Urbana-Champaign, Urbana, IL

[3]Howard Hughes Medical Institute, Baltimore, MD

[4]Department of Biophysics and Biophysical Chemistry, Department of Biophysics, Department of Biomedical Engineering, Baltimore, MD

[#] These authors contributed equally to this work.

## Abstract

Crystallography has provided invaluable insights to ion channel selectivity and gating, but to advance understanding to a new level, dynamic views of channel structures within membranes are essential. We labeled tetrameric KirBac1.1 potassium channels with single donor and acceptor fluorophores at different sites, and examined structural dynamics within lipid membranes by single molecule FRET. We found that the extracellular region is structurally rigid in both closed and open states, whereas the N-terminal slide helix undergoes marked conformational fluctuations. The cytoplasmic C-terminal domain fluctuates between two major structural states both of which become less dynamic and move away from the pore axis and away from the membrane in closed channels. Our results reveal mobile and rigid conformations of functionally relevant KirBac1.1 channel motifs, implying similar dynamics for similar motifs in eukaryotic Kir channels and for cation channels in general.

## Introduction

Since gated currents through single ion channel pores were first observed over 40 years ago[1], the gating behaviors of many ion channels have been recorded and analyzed at the single molecule level, and numerous kinetic schemes have been developed to predict



[#] Correspondence to TJH (; Email: tjha@jhu.edu) or CGN (; Email: cnichols@wustl.edu)

Author Contributions

SW, RV, TH and CGN conceived and designed the experiments; SW and WB performed the electrophysiological studies; SW designed, constructed, purified and labeled the protein samples with fluorophore, WB analyzed the single channel recordings, SW and RV collected and analyzed the smFRET data. The paper was written by SW and CGN, and edited by RV, WB and TH.

physical states underlying gating transitions[2]. Meanwhile, membrane protein crystallography has provided high resolution structures of ion channels in various configurations, and has suggested conformational changes that must occur for currents to turn on and off[3-7]. Crystal structures have led to ideas about structural mobility and rigidity, such as (1) the K channel selectivity filter is a rigid structural feature [8-10], (2) the slide helix of Kir channels[11-14], or the short α-helix that links the voltage sensor and the channel pore in voltage-gated channels, plays a role in controlling the helix bundle crossing (HBC) gate[15,16], and (3) the Kir channel cytoplasmic domain itself moves relative to the transmembrane domain during gating[4,17,18]. However, crystallographic analyses cannot test these ideas since they typically access only a few stable states of channel proteins and in environments that are very different from the lipid bilayer. Hence the relevance of crystallographic 'snapshots' to the dynamic gating events of ion channels in cell membranes may not always be apparent.

Inward rectifier potassium (Kir) channels play critical roles in shaping action potentials of cardiomyocytes, potassium homeostasis of the kidney, hormone secretion of pancreatic β-cells, membrane potentials of nerve and glial cells, as well as the electrical activity of endothelial and smooth muscle cells[19]. Multiple Kir channel structures have been resolved, but conformational trajectories of gating transitions remain speculative, although they are critical for a full understanding of gating mechanisms. KirBac1.1 is a prokaryotic Kir homolog which has the same core structural elements as eukaryotic Kir channels[17,20,21], and provides a model system to study Kir channel gating; both crystallographic and molecular simulation analyses indicate similar structures of open and closed channels in bacterial and eukaryotic Kir homologues[4,17,18,22]. Phosphatidylinositol 4,5-bisphosphate ($PIP_2$) is a gating ligand for many ion channels, and is a universal activatory ligand for eukaryotic Kir channels[23-25], stabilizing the open conformation[4,17,19,25]. In prokaryotic KirBac1.1, the $PIP_2$ binding site is not identical, resulting in a switched coupling whereby $PIP_2$ acts to stabilize the closed state[26].

Single molecule FRET (smFRET) can report unsynchronized conformational changes that are masked by ensemble averaging of macroscopic measurements[27,28], and may bridge the gap between crystal structures and single ion channel current analyses. Very few membrane proteins have been studied by smFRET[29-33] due to technical challenges of position-specific fluorophore labeling, particularly in multimeric proteins. In the present study, we have implemented the use of smFRET to analyze the dynamics of structural motions in KirBac1.1 in the closed ($PIP_2$ bound) and open (unliganded) states. The results reveal both flexible and rigid motifs of the channel, confirming and refuting previous ideas about structural mobility, as well as generating novel ideas regarding the structural dynamics of the gating transition itself in potassium channels.

## Results

### Labeled tetrameric KirBac1.1 for single molecule imaging

In liposomes of defined composition (POPE:POPG = 3:1) without $PIP_2$, KirBac1.1 channels exhibit spontaneous bursts of openings, but the channels are essentially completely closed after incorporation of $PIP_2$ (Fig. 1a,b, Supplementary Table 1). In the absence of $PIP_2$, three

distinct closed times are resolvable (Fig. 1c), and when open, the channels occupy two resolvable conductance levels (Fig. 1b) with similar durations. The mean probability of being in any open state ($P_o$) is ~0.12 under control conditions, and is reduced to ~0.004 in the presence of 5 μM $PIP_2$ (Fig. 1d).

We have successfully applied smFRET to KirBac1.1 channels by engineering, expressing, labeling, and reconstituting concatemeric proteins containing only 2 cysteines within the tetrameric channel (Fig.2a-c). Tetramer fractions of Alexa Fluor 555 and Alexa Fluor 647 c2 maleimide labeled KirBac1.1 mutants were collected by size exclusion chromatography (Supplementary Fig.1A) and reconstituted into liposomes (POPE:POPG = 3:1). Functional assays confirm that all labeled mutants retain channel activity and sensitivity to $PIP_2$ inhibition that is similar to WT (Supplementary Fig.1B). Single molecule imaging was performed with a prism-based TIRF microscope[28] with time resolution of 30ms and 100ms (Fig. 2d). The mutant proteins were labeled very specifically with over 95% fluorescent spots arising from KirBac1.1 cysteine mutants, in comparison with WT control (Fig.2e, Supplementary Fig.1C).

## Structural rigidity of the extracellular region

The backbone structure of the selectivity filter region is remarkably consistent in all crystallized K channels[7,8,34], but whether this simply reflects a stable crystallographic configuration, or a functionally relevant rigidity, is unknown. Computational and experimental analyses[35] suggest conformational coupling of the selectivity filter to the loop that extend outwards. To provide direct visualization of structural dynamics in the extracellular selectivity filter region (Fig. 3a), we labeled the residue T120C at the top of this loop in KirBac1.1. Individual smFRET trajectories reveal a remarkably stable FRET efficiency of ~0.8, without fluctuations, and which does not change when the channel is closed by saturating $PIP_2$ (Figs. 3a,b, Supplementary Fig. 2A, Supplementary Table 2). smFRET histograms and population contour plots obtained from 76 individual channel records in the absence of $PIP_2$ (and 91 in the presence of $PIP_2$) (Fig. 3b, as well as data acquired at 30 ms time resolution - Supplementary Fig.3A), confirm that FRET efficiencies at this position have a very narrow distribution which does not differ between closed and open states. These experiments provide a first time-resolved demonstration of the rigidity of the extracellular selectivity filter region, independent of the channel gating state, in functional channels embedded within a lipid membrane environment.

## Slide helix constriction in $PIP_2$

A ubiquitous structural motif of many K channels, the N-terminal amphipathic slide helix forms a ‘belt’ around the channel at the cytoplasmic face of the membrane and has been proposed as a key linking element between ligand-binding or voltage-sensing gating domains and the pore[16,36]. In Kir channels, the slide helix may participate in controlling the HBC gate, but structural mechanisms are not clear[4,17,21,37,38]. We placed FRET pairs in dimeric constructs at opposing A45C residues, located at the N-terminal ends of the slide helices (Fig. 2a,b). As shown by individual smFRET trajectories (Fig. 3c, Supplementary Fig. 2B), more than 50% of traces exhibit rapid fluctuations in FRET efficiencies between three major states both in the absence and the presence of $PIP_2$. The dimensionless variance

in fluorescence intensities of singly (Alexa555) labeled A45C-WT (8.7 ± 1.7) and T120C-WT (5.7 ± 1.2) samples were not significantly different, consistent with the measured FRET changes at residue 45 resulting from conformational changes, rather than changes in signal-noise ratio, or changes in local quantum efficiency.

smFRET contour plots and histograms from 121 individual recordings in the absence of $PIP_2$ (139 with $PIP_2$) (Fig. 3d, Supplementary Fig. 2B) reveal a distribution of FRET efficiencies between ~0.45 and ~0.95, suggesting a motion range up to 20 Å between diagonally opposed slide helices. (based on distances (r) calculated using the Förster equation: $r = R_0*(1/E-1)^{1/6}$, where $R_0$ is the Förster distance of the Alexa Fluor 555 and 647 FRET pair (5.1 nm), with the assumption that the fluorophores can freely rotate at the labeling site, i.e $\kappa^2 = 2/3$). The FRET efficiency distributions are well fit by the sum of 3 Gaussians (Fig. 3d, Table 1, Supplementary Table 2), without significant alteration in the histogram peak positions, with and without $PIP_2$. In the closed channel, individual trajectories (Fig. 2c, Supplementary Fig.2B), as well as histograms (Fig. 2d), reveal a marked increase in the fraction of highest (~0.87), and decrease in the fraction of lowest (~0.48) FRET efficiency populations (Table 1, Supplementary Table 2). If we make the simplistic assumption that channel opening requires both diagonally opposed A45C pairs to be in the most dilated conformation (FRET efficiency ~0.48), the predicted open probability would be the square of the occupancy of the $P_{0.48}$ state, i.e. 0.13 ($0.36^2$) in the absence of $PIP_2$, and 0.04 ($0.20^2$) in the presence of $PIP_2$. These values are quite similar to measured open probabilities (0.12 and 0.005, respectively, in Fig. 1d), but further work will be necessary to validate these ideas.

Independent sets of A45C-WT smFRET data collected at 30 ms resolution generated very similar distributions and recapitulated the $PIP_2$ effects on FRET distributions (Supplementary Fig.3a). Although the shorter inter-residue distance reduces the sensitivity of the Alexa fluor 555 and Alexa 647 pair, qualitatively similar gating-dependent FRET changes were also identified in data from W48C-WT, located in the middle of the slide helix (Supplementary Fig.3b). Our results thus implicate slide helix motions during channel gating and suggest that closure of the channel involves tightening of the slide helix ‘belt’, with the lowest FRET states corresponding to the ‘dilated’ belt that permits channel opening.

## Structural transitions in the C-terminal domain

Kir channels have a large C-terminal domain (CTD) with which many intracellular regulatory ligands interact[24]. We previously reported reduced ensemble FRET efficiency at the A273C position in the presence of $PIP_2$[22]. In the present study, we again labeled two cytoplasmic domain cysteines, F167C and A273C, and the external residue T120C with EDANS and DABCYL-plus or Alexa-Fluor-488 and QSY-7 FRET pairs in dimeric or tetrameric constructs, and measured the $PIP_2$-induced changes using ensemble FRET. Both 167C and 273C exhibited reduced FRET efficiencies with $PIP_2$, while there was no significant change in FRET efficiency at 120C (Supplementary Fig. 4A).

To visualize conformational dynamics of the CTD in closed and open states, we labeled diagonally opposed cysteines in the dimeric A273C-WT or F167C-WT constructs with Alexa Fluor 555 and Alexa Fluor 647 (Fig. 2a,b). As indicated by individual smFRET

trajectories (Fig. 3E, Supplementary Fig. 2c), more than 60% of A273-WT traces exhibited fluctuations between 2 major conformations with mean FRET efficiencies of 0.74 and 0.41 in the absence of $PIP_2$. In the presence of saturating $PIP_2$, the number of traces showing detectable dynamic changes was decreased to ~30% (Fig. 3e, Table 2), and both FRET peaks shifted towards lower FRET values of 0.68 and 0.32, respectively (Fig. 3f). These results are consistent with the ensemble FRET measurements, but further suggest that the β-sheet which contains residue 273 actually fluctuates between two major conformations whether the channel is closed or open, and that both conformations are widened when the channel is closed. At the F167 site, the smFRET distributions also exhibit two clear peaks in both the absence and presence of $PIP_2$, and again induces only a slight shift towards lower FRET efficiency (Supplementary Fig.3B). These data suggest that in addition to overall dilation in the closed channel, the major β-sheet in the CTD may undergo gating-independent 'breathing' conformational transitions that are not revealed in crystal structures.

## C-terminal displacement from the membrane in closed channels

Crystal structures of both potassium and sodium channels indicate that bending and rotation motions of the pore forming helices (TM2 or S6) are required to remove HBC gates[6,7,36,39]. For Kir channels, a rigidly coupled tilting or twisting of the CTD has also been proposed[4,18,22]. To test this idea directly, we constructed 3 concatemeric tetramers in which the channels were labeled across the membrane, at one cysteine in the selectivity filter region of extracellular side (T120C) and at A270C in the CTD of the same, the neighboring, or the diagonally opposed, subunit (Fig. 2c). smFRET trajectories, as well as FRET contour plots and histograms from these three constructs all indicate significant decrease in FRET efficiencies when the channels are closed by $PIP_2$ (Fig. 4, Supplementary Fig. 5A-C). Ensemble FRET data from the same constructs were again consistent with these calculated from smFRET measurements (Supplementary Fig. 4B). These data thus indicate that the CTD indeed moves away from the TM when the channel closes; FRET efficiencies are consistent with the channel being ~80 A long in the closed state, similar to the channel length observed in the 1P7B KirBac1.1 crystal structure[21], and becoming ~10 A shorter in the open state. This conclusion is consistent with those of other crystallographic and simulation studies[17,40], but does not support gating being associated with a major twisting motion of the CTD relative to the TM[41], since this would differentially affect the FRET signals in the three intra- or intersubunit arrangements.

## Relating structural dynamics to ion current gating

At location T120C in the extracellular portion of the channel near the selectivity filter, there are very few detectable dynamics, with over 90% of traces showing no change in FRET efficiency before donor or acceptor photo bleaching (Table 2), and no cross-correlation was detected between donor and acceptor signal (Fig. 5a). In contrast, A45C in the slide helix region exhibits a strong donor-acceptor cross-correlation with decay time constant that is not dramatically altered by $PIP_2$ (Fig. 5b). We propose that the structural dynamics at A45C are dominated by transitions among the multiple conformations of the closed state, and that channel opening may occur at the lowest FRET conformations (Fig. 3c,d). It is noteworthy that at the nearby residue W48C, the FRET signals are less dynamic (Supplementary Fig. 3B), which may be a consequence of each residue being located in different secondary

structures, or different local environments (i.e A45 is located just before the slide helix in a loop interacting with the CTD, and relatively more exposed to the cytoplasm, whereas W48 constitutes part of the slide helix itself, and sits at the cytoplasm-membrane interfacial region). Striking differences in FRET dynamics between active and closed channels were seen at residue A273 of the CTD (Figs. 3e, 5c). The donor-acceptor cross-correlation of the A273C-WT sample is well fit with a double exponential function, with both time constants significantly increasing in $PIP_2$, while the amplitude of both components decreases (Fig. 5c). These changes suggest that the frequency of the conformational fluctuations in this region are suppressed when the channel is closed, consistent with a model in which ionic current gating at the helix bundle crossing is directly coupled to conformational changes in the CTD[22].

## Discussion

Crystal structures provide images of channels in distinct states, but cannot reveal the connectivity between states nor provide time trajectories of structural changes. Our detection of unsynchronized structural dynamics using smFRET provides a first observation of the intra-molecular motions that underlie Kir channel function within lipid membranes.

Certain findings are quite striking and likely to have significant implications for other channels. Perhaps most notably, the external selectivity filter region exhibits no detectable structural fluctuations, demonstrating a rigidity that may be necessary to maintain ion selectivity of the pore. In contrast, both the slide helix and the CTD show marked structural dynamics and structural flexibility. Our results suggest that the tightness of the slide helix 'belt' controls channel gating (Fig. 5d). In KirBac1.1 the 'belt' is tightened by $PIP_2$ binding, a structural consequence that may be reversed for eukaryotic Kir channels in which a structurally distinct slide-helix is involved in $PIP_2$–dependent activation [17]. The motions we detect in the KirBac1.1 slide helix and CTD reflect a marked intrinsic flexibility of the channel structure. As more ion channels become amenable to similar approaches to those we describe here, we envision that the conformational changes induced by gating processes in eukaryotic Kir and other ion channels may be revealed to be more dramatic and more complex than currently perceived.

## Online Methods

### DNA manipulation

KirBac1.1 WT cDNA was inserted between NcoI and HindIII sites of the pQE60 vector[43]. For tandem dimer constructs, two copies of KirBac1.1 cDNA were inserted between NcoI and BamHI, BamHI and HindIII sites, respectively. A short 'GlyGlyGlySerGlyGlyGlySer ' linker was introduced between the two copies of KirBac1.1 coding DNA. To make tandem tetramer constructs, two copies of tandem dimer coding DNA were inserted between NcoI and SacI, SacI and HindIII of the pET28a(+) vector with a 'GlyGlyGlySerGlyGlyGlySer ' linker between them. In tandem constructs, all mutations were introduced into the KirBac1.1 monomer plasmid first by site-direct mutagenesis kit (Agilent Inc.), and then subcloned into the tandem dimer or tetramer constructs. A 8xHis tag was introduced in the C-termini of all the protomers for metal affinity purification.

### Protein expression and purification

KirBac1.1 WT protein was expressed in BL21-Gold (DE3)-pLysS host strain, after induction by 1.0 mM IPTG for 3 hrs at 37 °C when the OD600 reached 0.8~1.0. KirBac1.1 tandem dimer or tetramer constructs were expressed in the BL21-Gold (DE3) host strain, and cultures were induced by 0.1 mM IPTG overnight at 20 °C when the OD600 reached about 0.6~0.8. Metal affinity purification was performed as described previously[43,44]. Affinity purified proteins were loaded onto a gel filtration column (Superdex-200, GE Healthcare Inc.) and tetramer fractions were collected for the following functional or structural studies.

### Protein labeling

Tetramer fractions of KirBac1.1 proteins were concentrated to 1 mg/ml in labeling buffer containing 20 mM Hepes, 150 mM KCl, 5 mM DM, pH7.0. A 1:1 mixture of Alexa Fluor 555 and 647 c2 maleimide were added into the protein solution at protein:fluorophore ratio of 1:4. Labeling reactions were conducted at room temperature for 2 hrs, then terminated by 10 mM β-mercaptoethanol and incubated at room temperature for an additional 30 min. Labeled proteins were diluted 10× in labeling buffer and then mixed with Cobalt Affinity Resin (Clonetech Inc). Free fluorophores were completely removed by extensive washing (>100 bed volumes) and protein was eluted by elution buffer (20 mM HEPES, 150 mM KCl, 5 mM DM, 400 mM imidazole, pH7.5). Eluted proteins were loaded on a gel filtration column (Superdex-200 10/30, GE Healthcare) and tetramer fractions were collected and concentrated for rubidium flux assay or single molecule imaging experiments.

### Rubidium flux assay

Purified KirBac1.1 proteins were reconstituted into POPE:POPG (3:1) liposomes with or without 1% (w/w) $PIP_2$, at protein:lipid ratio of 1:100. The protein and lipid mixtures were incubated for 20 min under room temperature and proteoliposomes were formed by removing the detergent with Sephadex G-50 spin columns. Rubidium flux assays were performed on proteoliposome samples as described previously[22,44]. Rubidium uptake of all mutants was normalized against WT protein in liposomes without $PIP_2$. We used purified $PIP_2$ from brain (Avanti cat#840046P), which was mixed with either K-MOPS buffer for rubidium flux assays and single channel recordings, or with K-HEPES-TROLOX buffer for single molecule imaging with the final predicted nominal concentration of 5 or 100 μM. $PIP_2$ likely assembles into micelles and then incorporates into liposomes by micelle fusion which cannot be washed away.

### Single channel recordings

Single channel recordings were performed on reconstituted WT KirBac1.1 in giant liposomes as previously described[20]. Excised inside-out patch recordings were performed with electrodes of 2-5 MΩ and symmetrical bath and pipette solutions consisting of (in mM) 20 MOPS, 158 KCl, and adjusted to pH 7.5 (KOH) were used. Single channel current responses were measured at an applied membrane potential of −100 mV, amplified and low-pass filtered at 1 kHz, sampled at 10 kHz (Axopatch 1B, 4-pole Bessel), converted into

digital files in Clampex7, and stored on an external hard drive for offline analysis using QuB kinetic software (www.qub.buffalo.edu).

## Single molecule Imaging

KirBac1.1 tandem proteins labeled with Alexa Fluor 555 and 647 were mixed with lipids (10 mg/ml, POPE:POPG = 3:1, 2% biotinylated-POPE, in buffer containing 20 mM HEPES, 150 mM KCl, 1 mM EDTA, 1 mM EGTA, 35 mM CHAPS, pH7.5) at protein:lipid ratio of 1:200 (w:w). The mixtures were incubated for 20 min at room temperature and proteliposomes were formed by removing the detergent with Sephadex G-50 spin columns. Proteoliposomes were diluted 10-50 times with reconstitution buffer (20 mM Hepes, 150 mM KCl, 1 mM EDTA, 1 mM EGTA, pH7.5), loaded into a PEGylated sample chamber and immobilized on the surface through neutravidin[45]. Single molecule imaging was performed on a prism-based TIRF microscope with 532 nm laser as excitation light. At the beginning or end of single molecule imaging, 640 nm excitation was also used to confirm the existence of acceptor fluorophore, particularly for constructs with low FRET efficiencies. The imaging buffer contained 20 mM HEPES, 150 mM KCl, 1 mM EDTA, 1 mM EGTA, ~3 mM Trolox, 1 mM 4-nitrobenzyl alcohol (NBA) and 1 mM cyclooctatetraene (COT), pH7.5. After collecting single molecule imaging data in control condition (without $PIP_2$), the imaging buffer was replaced with $PIP_2$-containing buffer (imaging buffer with additional 100 μM $PIP_2$). After 5 min of incubation, the sample chamber was flushed again with $PIP_2$ imaging buffer, then single molecule images were collected following the same procedure as that for control condition.

## Data analysis

**Single channel recordings—**Preprocessing and analyses of single channel current recordings were performed offline with QuB software (www.QuB.Buffalo.edu). Brief (< 9 samples) current spikes during prolonged closures were adjusted to the adjacent non-conducting current amplitude to eliminate infrequent electrical noise and instances of baseline drift were corrected by setting the baseline to an initial zero-current level through the use of baseline nodes. Current amplitudes were estimated from preprocessed data with the 'AMP' function that utilizes the Baum-Welch re-estimation algorithm and were typically well described by three Gaussian components corresponding to one non-conducting and two resolvable conducting amplitudes. Whole file recordings were digitally low-passed filtered at 400 Hz and idealized using a 50% threshold method using the corresponding single-channel amplitudes with no imposed dead time. The resulting idealization was inspected by visual comparison to that of the digitally filtered current signal. Interval distributions were typically well fit with three closed components and one open component for each open conductance class..

**Single molecule FRET data analysis—**The movies acquired in single molecule imaging were processed with an IDL script (available on request) to identify and extract donor and acceptor fluorescence intensity profiles of individual molecules[28]. Traces extracted from the movies were interactively selected, with the following acceptance criteria: (1) No more than one bleaching step for both donor and acceptor fluorophores; (2) The donor and acceptor fluorescence intensities showed clear anti-correlated pattern; (3) The

total fluorescence intensity from donor and acceptor was constant before photo bleaching occurred; (4) The lifetime of both donor and acceptor fluorophore were longer than 5s. All analyzed smFRET traces were selected independently by two analysts (SW and RV), and then analyzed following the same algorithm. No significant difference were found between the traces selected by SW and RV.

The bin size of all histograms was set as 0.02. FRET histograms of each single trace, regardless of length, was normalized to total counts (i.e. every trace contributed equally to the final histograms, to avoid dominant effects of long traces). The final histograms were obtained by combining the FRET histograms of each trace and then re-normalizing against total counts. To generate FRET contour plots, the first 5 sec of data from each trace was extracted and the histogram at each time point was obtained and normalized to total counts. The normalized coefficients of cross-correlation were calculated using the 'xcov' function (Signal Processing Toolbox) in Matlab©. The maximum lag was 20 sec and traces shorter than 20 sec were excluded from the analysis. The cross-correlation data were fitted with a two component exponential function using curve-fitting tool box in Matlab©.

Calculated time constants and areas for individual exponential components were tabulated and reported as means ± SE.

## Supplementary Material

Refer to Web version on PubMed Central for supplementary material.

## Acknowledgements

Financial support was provided by NIH Grant HL54171 (CGN) and NSF grant PHY1430124 (TJH). TJH is supported as an investigator with the Howard Hughes Medical Institute. WB was supported by NIH T32 HL007275 and T32 HL125241.

## References

1. Neher E, Sakmann B. Single-channel currents recorded from membrane of denervated frog muscle fibres. Nature. 1976; 260:799–802. [PubMed: 1083489]
2. Colquhoun, D.; Sigworth, F. Single-channel recording. Springer; US: 1995. Fitting and statistical analysis of single-channel records.; p. 483-587.
3. Cao E, Liao M, Cheng Y, Julius D. TRPV1 structures in distinct conformations reveal activation mechanisms. Nature. 2013; 504:113–8. [PubMed: 24305161]
4. Whorton MR, MacKinnon R. Crystal structure of the mammalian GIRK2 K+ channel and gating regulation by G proteins, PIP2, and sodium. Cell. 2011; 147:199–208. [PubMed: 21962516]
5. Cuello LG, Jogini V, Cortes DM, Perozo E. Structural mechanism of C-type inactivation in K(+) channels. Nature. 2010; 466:203–8. [PubMed: 20613835]
6. Cuello LG, et al. Structural basis for the coupling between activation and inactivation gates in K(+) channels. Nature. 2010; 466:272–5. [PubMed: 20613845]
7. Jiang Y, et al. Crystal structure and mechanism of a calcium-gated potassium channel. Nature. 2002; 417:515–22. [PubMed: 12037559]
8. Zhou Y, Morais-Cabral JH, Kaufman A, MacKinnon R. Chemistry of ion coordination and hydration revealed by a K+ channel-Fab complex at 2.0 A resolution. Nature. 2001; 414:43–8. [PubMed: 11689936]

9. Nordengren J, et al. Differential localization and expression of urokinase plasminogen activator (uPA), its receptor (uPAR), and its inhibitor (PAI-1) mRNA and protein in endometrial tissue during the menstrual cycle. Molecular human reproduction. 2004; 10:655–63. [PubMed: 15243126]
10. Berneche S, Roux B. Energetics of ion conduction through the K+ channel. Nature. 2001; 414:73–7. [PubMed: 11689945]
11. Nichols CG. KATP channels as molecular sensors of cellular metabolism. Nature. 2006; 440:470–6. [PubMed: 16554807]
12. Enkvetchakul D, Jeliazkova I, Bhattacharyya J, Nichols C. Control of inward rectifier K channel activity by lipid tethering of cytoplasmic domains. The Journal of general physiology. 2007; 130:329–334. [PubMed: 17698595]
13. Mannikko R, et al. Interaction between mutations in the slide helix of Kir6.2 associated with neonatal diabetes and neurological symptoms. Human molecular genetics. 2010; 19:963–72. [PubMed: 20022885]
14. Kuo A, Domene C, Johnson LN, Doyle DA, Venien-Bryan C. Two different conformational states of the KirBac3.1 potassium channel revealed by electron crystallography.[see comment]. Structure. 2005; 13:1463–72. [PubMed: 16216578]
15. Lu Z, Klem AM, Ramu Y. Coupling between voltage sensors and activation gate in voltage-gated K+ channels. Journal of General Physiology. 2002; 120:663–76. [PubMed: 12407078]
16. Long SB, Campbell EB, Mackinnon R. Voltage sensor of Kv1.2: structural basis of electromechanical coupling. Science. 2005; 309:903–8. [PubMed: 16002579]
17. Hansen SB, Tao X, MacKinnon R. Structural basis of PIP2 activation of the classical inward rectifier K+ channel Kir2.2. Nature. 2011; 477:495–8. [PubMed: 21874019]
18. Bavro VN, et al. Structure of a KirBac potassium channel with an open bundle crossing indicates a mechanism of channel gating. Nature structural & molecular biology. 2012; 19:158–63.
19. Hibino H, et al. Inwardly rectifying potassium channels: their structure, function, and physiological roles. Physiological reviews. 2010; 90:291–366. [PubMed: 20086079]
20. Cheng WW, Enkvetchakul D, Nichols CG. KirBac1.1: it's an inward rectifying potassium channel. The Journal of general physiology. 2009; 133:295–305. [PubMed: 19204189]
21. Kuo A, et al. Crystal structure of the potassium channel KirBac1.1 in the closed state. Science. 2003; 300:1922–6. [PubMed: 12738871]
22. Wang S, Lee SJ, Heyman S, Enkvetchakul D, Nichols CG. Structural rearrangements underlying ligand-gating in Kir channels. Nature communications. 2012; 3:617.
23. Suh BC, Hille B. PIP2 is a necessary cofactor for ion channel function: how and why? Annual review of biophysics. 2008; 37:175–95.
24. Xie LH, John SA, Ribalet B, Weiss JN. Activation of inwardly rectifying potassium (Kir) channels by phosphatidylinositol-4,5-bisphosphate (PIP2): interaction with other regulatory ligands. Progress in biophysics and molecular biology. 2007; 94:320–35. [PubMed: 16837026]
25. Logothetis DE, Jin T, Lupyan D, Rosenhouse-Dantsker A. Phosphoinositide-mediated gating of inwardly rectifying K(+) channels. Pflugers Archiv : European journal of physiology. 2007; 455:83–95. [PubMed: 17520276]
26. Enkvetchakul D, Jeliazkova I, Nichols CG. Direct modulation of Kir channel gating by membrane phosphatidylinositol 4,5-bisphosphate. The Journal of biological chemistry. 2005; 280:35785–8. [PubMed: 16144841]
27. Ha T, et al. Probing the interaction between two single molecules: fluorescence resonance energy transfer between a single donor and a single acceptor. Proceedings of the National Academy of Sciences of the United States of America. 1996; 93:6264–8. [PubMed: 8692803]
28. Roy R, Hohng S, Ha T. A practical guide to single-molecule FRET. Nature methods. 2008; 5:507–16. [PubMed: 18511918]
29. Zhao Y, et al. Single-molecule dynamics of gating in a neurotransmitter transporter homologue. Nature. 2010; 465:188–93. [PubMed: 20463731]
30. Akyuz N, Altman RB, Blanchard SC, Boudker O. Transport dynamics in a glutamate transporter homologue. Nature. 2013; 502:114–8. [PubMed: 23792560]

31. Erkens GB, Hanelt I, Goudsmits JM, Slotboom DJ, van Oijen AM. Unsynchronised subunit motion in single trimeric sodium-coupled aspartate transporters. Nature. 2013; 502:119–23. [PubMed: 24091978]
32. Wang Y, et al. Single molecule FRET reveals pore size and opening mechanism of a mechano-sensitive ion channel. eLife. 2014; 3:e01834. [PubMed: 24550255]
33. Vafabakhsh R, Levitz J, Isacoff EY. Conformational dynamics of a class C G-protein-coupled receptor. Nature. 2015; 524:497–501. [PubMed: 26258295]
34. Roux B. Ion conduction and selectivity in K(+) channels. Annual review of biophysics and biomolecular structure. 2005; 34:153–71.
35. Raghuraman H, Islam SM, Mukherjee S, Roux B, Perozo E. Dynamics transitions at the outer vestibule of the KcsA potassium channel during gating. Proceedings of the National Academy of Sciences of the United States of America. 2014; 111:1831–6. [PubMed: 24429344]
36. Payandeh J, Scheuer T, Zheng N, Catterall WA. The crystal structure of a voltage-gated sodium channel. Nature. 2011; 475:353–8. [PubMed: 21743477]
37. Xiao J, Zhen XG, Yang J. Localization of PIP2 activation gate in inward rectifier K+ channels. Nature neuroscience. 2003; 6:811–8. [PubMed: 12858177]
38. Lee SJ, et al. Secondary anionic phospholipid binding site and gating mechanism in Kir2.1 inward rectifier channels. Nature communications. 2013; 4:2786.
39. McCusker EC, et al. Structure of a bacterial voltage-gated sodium channel pore reveals mechanisms of opening and closing. Nature communications. 2012; 3:1102.
40. Bollepalli MK, et al. State-dependent network connectivity determines gating in a K+ channel. Structure. 2014; 22:1037–46. [PubMed: 24980796]
41. Clarke OB, et al. Domain reorientation and rotation of an intracellular assembly regulate conduction in Kir potassium channels. Cell. 141:1018–29. [PubMed: 20564790]
42. Joo C, Ha T. Prism-type total internal reflection microscopy for single-molecule FRET. Cold Spring Harbor protocols 2012. 2012

## References for Online Methods

43. Enkvetchakul D, et al. Functional characterization of a prokaryotic Kir channel. The Journal of biological chemistry. 2004; 279:47076–80. [PubMed: 15448150]
44. Wang S, Alimi Y, Tong A, Nichols CG, Enkvetchakul D. Differential roles of blocking ions in KirBac1.1 tetramer stability. The Journal of biological chemistry. 2009; 284:2854–60. [PubMed: 19033439]
45. Joo C, Ha T. Preparing sample chambers for single-molecule FRET. Cold Spring Harbor protocols. 2012; 2012:1104–8. [PubMed: 23028078]

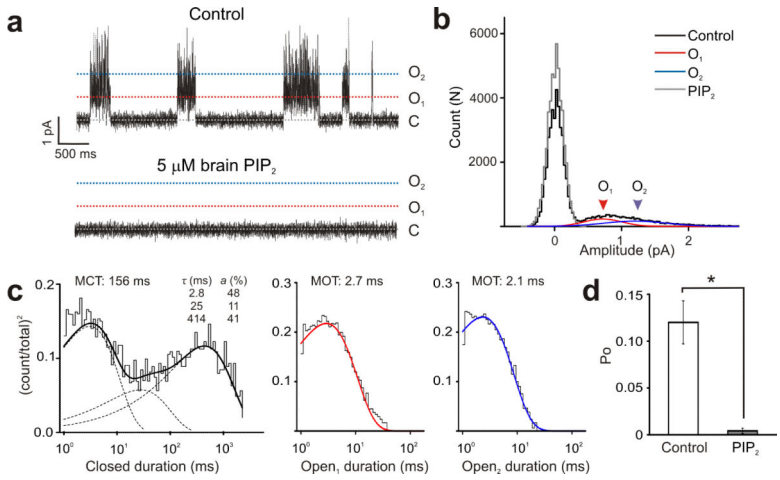


**Fig. 1. $PIP_2$ –dependent gating of KirBac1.1 channel activity**

(**a**) Representative excised single channel current traces of purified KirBac1.1 reconstituted into giant liposomes, before and after application of $PIP_2$. (**b**) Amplitude histogram of the corresponding traces in A before (black) and after applying (gray) $PIP_2$. (**c**) Closed and open interval distributions from the recording depicted in A, before $PIP_2$. Histograms are overlaid with the probability density function (thick lines) and individual exponential components (dotted lines). Mean closed (MCT) and open (MOT) times, time constants (τ, ms), and corresponding areas (*a*, %) were calculated from fits with a model consisting of three closed states and one open state for each conductance class. (**d**) Open probability ($P_O$, Mean + s.e.m.) in the absence (0.12 ± 0.02, n =5) and presence (0.004 ± 0.002, n=3) of $PIP_2$ (*, $p < 0.05$, Student's *t*-test).

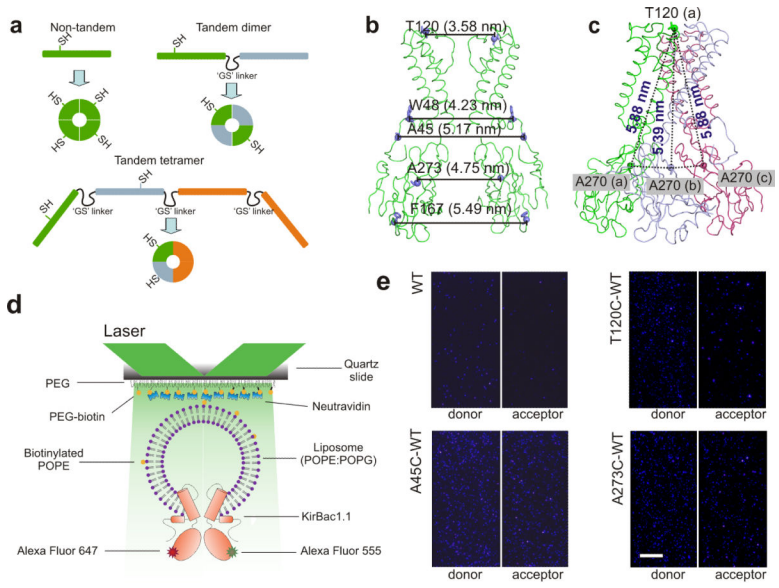


**Fig. 2. smFRET measurements of KirBac1.1 channel in liposomes**

(**a**) Strategy for introducing two free cysteines within tetrameric KirBac1.1 channel. The upper panels show the organization of the encoding cDNA, and lower panels are the domain organizations of the resulting proteins. Every ‘GS’ linkers contain 2 ‘GGGS’ amino acid repeats. (**b,c**) Fluorophore-labeled positions in KirBac1.1 tandem dimer and tetramer constructs. (**d**) Prism-based TIRF setup to perform single molecule imaging on KirBac1.1 reconstituted into liposomes. (**e**) Representative images of single molecule imaging acquired with prism-based TIRF microscope [28,42]. The donor and acceptor emission channels are marked by solid blue and red boxes. Scale bar represents 5μm.

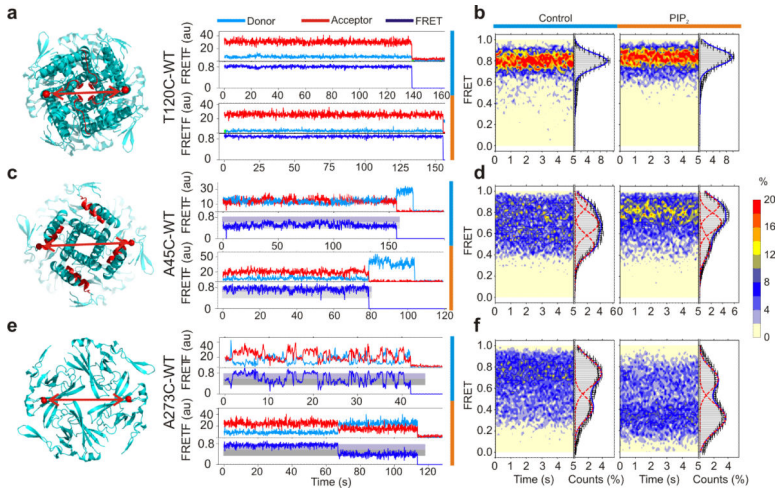


**Fig. 3. Conformational fluctuations of KirBac1.1 in liposomes**

Labeling locations and representative smFRET traces for residues T120C (**a**), A45C (**c**) and A273F (**e**), as well as FRET contour plots and histograms (**b**, **d** and **f**, mean + s.e.m., n = 76 and 91 T120 traces, 121 and 139 A45C traces, and 175 and 204 A273C traces, in the absence and presence of $PIP_2$, respectively) of KirBac1.1 in liposomes with (red bars) or without $PIP_2$ (blue bars).

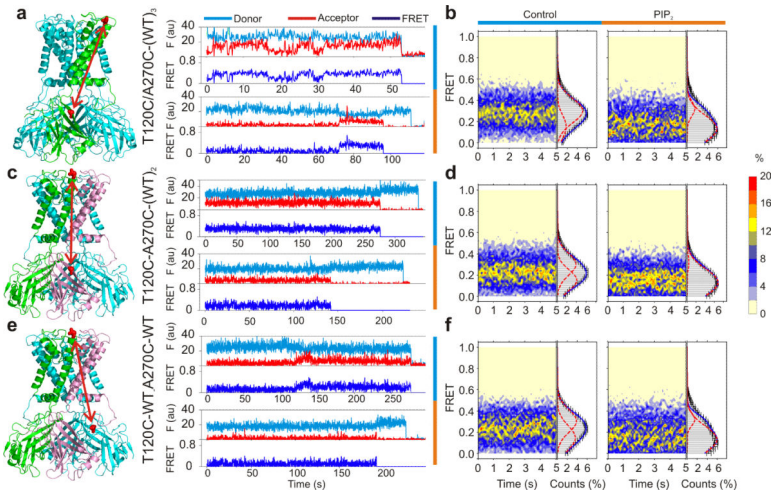


**Fig. 4. Motion of the TM with respect to CTD upon $PIP_2$ gating**

Labeling locations and representative smFRET traces for T120-A273C residue pairs, with A273C located in the same subunit (**a**), the clockwise preceding residue (**c**) or the diagonally opposite subunit (**e**), as well as FRET contour plots and histograms (b, **d** and **f**) of KirBac1.1 in liposomes with (orange bars) or without $PIP_2$ (blue bars) (mean + s.e.m., n = 149-267 traces in each case).

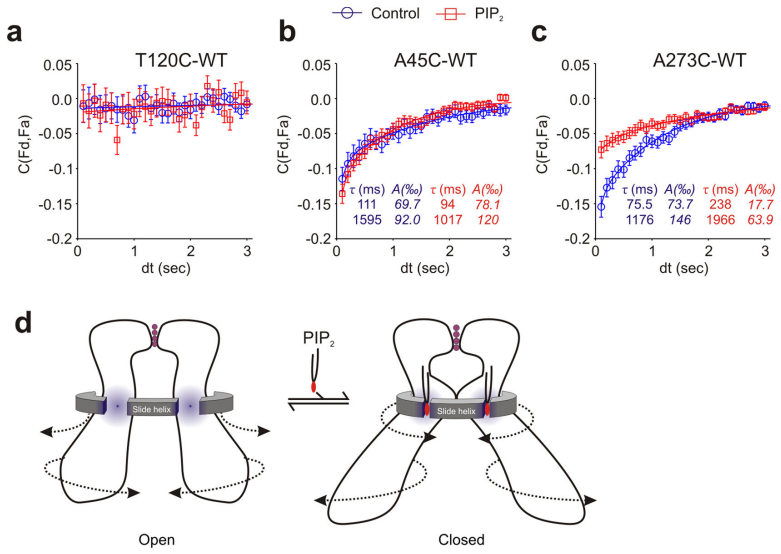


**Fig. 5. Conformational dynamics of KirBac1.1 and $PIP_2$–dependent gating**

Cross-correlation (C) of donor (Fd) and acceptor (Fa) fluorescence traces of KirBac1.1 mutants with fluorophore labeling at (**a**) T120C near the selectivity filter, (**b**) A45C in the slide helix, (**c**) A273C in the CTD, in the absence and presence of $PIP_2$, respectively (mean + s.e.m., n = 79-204 traces in each case). Fitted time constant (τ) and amplitude (A) are indicated in each case. (**d**) Proposed motions underlying gating of the KirBac1.1 channel. $PIP_2$ binds at the TM-CTD interface to tighten the slide helix 'belt' and confine the channel pore opening. Tilting or twisting motions of the CTD couple to the helix bundle crossing gate closure, slowing down structural fluctuations of the CTD.

**Table 1**

FRET populations at A45C position from Gaussian fittings

| A45C-WT | | $F_{0.87}$ | $F_{0.70}$ | $F_{0.48}$ | $F_{0.48}^2$ | $P_{o\ (SCR)}$ |
|---|---|---|---|---|---|---|
| Control | 100ms | 0.21 | 0.43 | 0.36 | 0.130 | 0.12 |
| | 30ms | 0.23 | 0.41 | 0.36 | 0.130 | |
| $PIP_2$ | 100ms | 0.34 | 0.44 | 0.22 | 0.048 | 0.004 |
| | 30ms | 0.36 | 0.44 | 0.20 | 0.040 | |

$F_X$ is the fraction of FRET distribution at efficiency = x. $P_O$ is the channel open probability.

## Table 2

Effect of $PIP_2$ on structural dynamics of KirBac1.1 evaluated by cross-correlation analysis[#]

| | | a1 (% ) | τ1 (ms) | a2 (% ) | τ2 (ms) | Dynamic traces[##] |
|---|---|---|---|---|---|---|
| T120C-WT | Control | - | - | - | - | 0.09 |
| | $PIP_2$ | - | - | - | - | 0.03 |
| A45C-WT | Control | 69.7 | 111 | 92.0 | 1595 | 0.55 |
| | $PIP_2$ | 78.1 | 94 | 120 | 1017 | 0.64 |
| A273C-WT | Control | 73.7 | 75.5 | 146 | 1176 | 0.60 |
| | $PIP_2$ | 17.7 | 238 | 63.9 | 1966 | 0.33 |

$$C_{auto}(t) = <\Delta fret_0 \Delta fret_t> / <\Delta fret_0^2> |$$

Where $\Delta fret_0$ and $\Delta fret_t$ are variance of FRET efficiencies at time 0 and t, respectively.

The cross-correlation analysis was performed with following algorithm:

$$C_{cross}(t) = <\Delta Fd_0 \Delta Fa_t> / <\Delta Fd_0 \Delta Fa_0>$$

Where $\Delta Fd_0$, $\Delta Fa_0$ and $\Delta Fa_t$ are variances of donor and acceptor fluorescence at time 0 and t, respectively.

All lag time (t) vs coefficients from cross co-variance analyses were fitted with either single- or two-component exponential functions:

$$f(C_{auto}, t) = a_1 e^{-\frac{t}{\tau 1}} + a_2 e^{-\frac{t}{\tau 2}} | \quad \text{or} \quad f(C_{auto}, t) = a_1 e^{-\frac{t}{\tau 1}}$$

[#]The cross-correlation analysis was performed with following algorithm:

[##]The FRET efficiency histogram of any trace exhibiting more than 1 population was arbitrarily defined as dynamic, in order to provide a semi-quantitative assessment of the dynamic behaviors of the labeled structural motifs.